Poincaré analysis of wave motion in ultrarelativistic electron-ion plasmas

G. Lehmann and K. H. Spatschek
Institut für Theoretische Physik, Heinrich-Heine-Universität Düsseldorf D-40225 Düsseldorf, Germany
(Received 27 August 2010; published 2 March 2011)

Based on a relativistic Maxwell-fluid description, the existence of ultrarelativistic laser-induced periodic waves in an electron-ion plasma is investigated. Within a one-dimensional propagation geometry nonlinear coupling of the electromagnetic and electrostatic components occurs that makes the fourth-order problem nonintegrable. A Hamiltonian description is derived, and the manifolds of periodic solutions are studied by Poincaré section plots. The influence of ion motion is investigated in different intensity regimes. For ultrarelativistic laser intensities the phase-space structures change significantly compared to the weakly relativistic case. Ion motion becomes very important such that finally electron-ion plasmas in the far-ultrarelativistic regime behave similarly to electron-positron plasmas. The characteristic new types of periodic solutions of the system are identified and discussed.

DOI: 10.1103/PhysRevE.83.036401 PACS number(s): 52.38.−r, 52.27.Ny, 52.35.Mw

I. INTRODUCTION

In parallel to the progress in laser technology, during the last decade research in relativistic plasma dynamics has been progressing significantly. Many new phenomena appear in the ultrarelativistic laser-plasma-interaction regime [1,2]. Intensities of 10^{19} Watt/cm^2 are now available in terawatt tabletop laser systems based on chirped-pulse amplification. In that regime, e.g., for circular polarization and wavelength $\lambda = 1\mu$m, the squared amplitude of the normalized laser vector potential (see below) may be of order 10 and higher. The relativistic γ factor for electrons then becomes much larger than 1, and clearly ultrarelativistic effects start dominating the nonlinear plasma dynamics.

Originally, the relativistic laser-plasma regime was analyzed in the classical paper by Akhiezer and Polovin [3], and later by Dawson and Kaw [4,5]. It was shown that the laser can generate longitudinal plasma waves due to the Lorentz force $q\vec{v} \times \vec{B}$, where q is the charge and $\vec{v}$ the velocity of the particle in the strong magnetic wave field $\vec{B}$. Relativistic coupling between transverse and longitudinal oscillations occurs. An interesting phenomenon in the new field of relativistic optics [2] is the completely different particle motion in relativistic waves compared to the well-known quiver motion in nonrelativistic oscillations. In linearly polarized laser light "figure-eight" orbits [6] appear as new solutions of the single-particle orbits in the average rest frame (where the average momentum is zero). The systematic understanding of periodic plasma motion in weakly relativistic waves persistently grew. The analysis is by far not trivial because of the nonlinear nature of the problem. Nonintegrability complicates the understanding of the complex dynamics. Not only regular but also chaotic solutions occur. Since the basic equations are in general not integrable, only in some limiting cases can analytical work be done. Akhiezer and Polovin [3] found exact solutions in the form of elliptic functions when no electromagnetic wave is present. For normalized phase velocities (see below) $\beta \equiv v/c \geqslant 1$ a second kind of solution has been identified analytically, first by Akhiezer and Polovin for $\beta \to \infty$, then in more general form for $\beta \geqslant 1$ by Kaw and Dawson [5], Max and Perkins [7], and Chian and Clemmow [8]. These solutions are linearly polarized and almost transverse. They have a small parallel momentum, which has twice the frequency of the transverse momentum. In the average drift (rest) frame, the fluid elements perform a motion along an eightlike trajectory in the plane spanned by propagation and polarization direction. Analytical results for this motion have been derived in the cases of $\beta \approx 1$ and $\beta \to \infty$ for weakly relativistic and ultrarelativistic waves [5,7–11]. Another possible periodic solution describes a circular trajectory, which also has already been noted by Akhiezer and Polovin [3]. It has been studied in more detail by Clemmow *et al.* [12,13], Bisai *et al.* [14], and Pesch and Kull [11]. For these solutions the parallel and the longitudinal momenta are of the same order of magnitude and have the same frequency. The solutions exist below and above the critical plasma density; the plasma density region is different from that for the figure-eight motion. Above the critical density circular trajectories are purely electrostatic, below the critical density an additional electromagnetic component is present. In addition to purely numerical solutions approximate analytical methods [15–18] also have been applied to discuss the various forms of the solutions.

It was demonstrated [19–21] that the systematic analysis of coupled transverse-longitudinal oscillations benefits from the methods that generally have been developed for nonlinear systems. As is known from other fields of nonlinear dynamics, Poincaré surface plots are very useful tools for characterizing the bifurcation scenarios in Hamiltonian systems. This is of particular importance in the presence of several control parameters. For example, phase velocity of the wave, plasma density, or laser amplitude may serve as control parameters, which together make the complex nonlinear problem rather confusing and rather unmanageable when no advanced nonlinear dynamics methods are being applied. As a particular result that has been obtained from studies of Poincaré surface plots we mention the disappearance of circular solutions for small plasma densities and the appearance of new types of solutions in the weakly relativistic regime within windows of plasma density [22].

Nonrelativistic models for high-frequency plasma waves treat ions as immobile without noticeable changes compared to an exact treatment with mobile ions. The reason is the small mass ratio $\epsilon_i = m_e/m_i$ (determined from the rest masses for

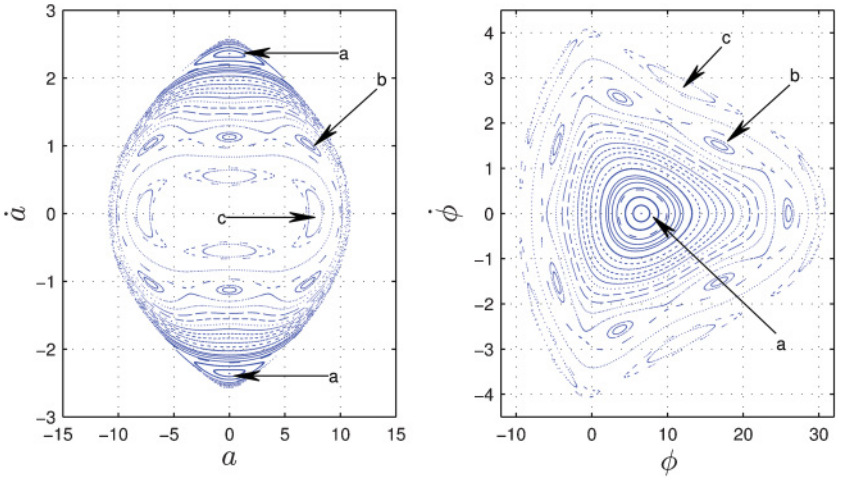

FIG. 1. (Color online) Poincaré surface plot of $\dot{a}$ versus a (for $\phi = \phi_{\min}$) and $\dot{\phi}$ versus ϕ (for $a = 0, \dot{a} > 0$), for $H = 10$ and $\beta = 2$ with mobile ions. Labeled are the fixed point a and the island chains b,c, corresponding to periodic wave motions.

electrons m_e and ions m_i). The ratio is largest for protons, i.e., $\epsilon_i \approx 1/1836 \ll 1$. However, it is well known that masses increase with increasing Lorentz factor γ caused by the quiver velocities of the particles. Since generally the electron quiver velocity is faster than that of ions, the electron γ factor γ_e increases faster than the ion γ factor γ_i. Therefore, for very large quiver velocities (or large laser amplitudes) $m_e\gamma_e/m_i\gamma_i \to 1$. In the latter case, ions (protons) should effectively behave like positrons when compared to electrons. Obviously, ion motion should no longer be neglected [23,24]. It is this effect that will be investigated in the present paper with respect to the existence of ultrarelativistic plasma waves.

To identify solutions and to understand the bifurcation scenario, i.e., the appearance of new solutions when changing the control parameter H (energy), we will make use of Poincaré surface section plots. As we shall show, the basic equations identify trajectories in a four-dimensional phase space of which we will render projections in order to identify the relevant structures. The trajectories are calculated from coupled oscillator equations by standard Runge-Kutta-methods. One of the oscillators will serve as a clock, while plotting the coordinates of the other one. The numerical methods used in the present work are described, e.g., in Refs. [25–27]. By this method it is easy to identify periodic solutions.

The manuscript is organized as follows. Section II summarizes results for stationary linearly polarized wave solutions from models with immobile ions. Section III discusses electron-ion plasmas with mobile ions and their influences on the dynamics in different energy regimes. The ultrarelativistic results for electron-ion plasmas will be compared with the phenomena in electron-positron plasmas in Sec. IV. For completeness, wave solutions in electron-positron-ion plasmas are also discussed. The paper is concluded by a short summary and discussion.

II. HAMILTONIAN SYSTEM FOR PLASMA WAVES WITH IMMOBILE IONS

Analytically, the problem of relativistic waves in plasmas is mostly treated within Maxwell-fluid models in a one-dimensional propagation geometry. Due to relativistic nonlinearities longitudinal electrostatic and transversal electromagnetic oscillations are coupled. The typical approach to derive coupled wave solutions is to look for stationary solutions in a frame of reference $\xi = x - vt$ moving with the normalized phase velocity $\beta = v/c > 1$ where c is the vacuum speed of light. In Appendix A we have formulated the equations of motion for the normalized laser vector potential a and the normalized scalar potential ϕ appearing due to the plasma reaction. We shall discuss now the nonlinear dynamics that is hidden in these equations.

For immobile ions, the equations of motion are

$$\frac{d^2a}{d\xi^2} = -a\frac{\beta}{\beta^2-1}\frac{1}{R_e}, \tag{1}$$

$$\frac{d^2\phi}{d\xi^2} = \frac{-\beta}{\beta^2-1}\left(\frac{\psi_e}{R_e} - \frac{1}{\beta}\right). \tag{2}$$

For the definition of $\psi_e \equiv \psi_e(\phi)$ and $R_e \equiv R_e(a,\phi)$ see Appendix A. Equations (1) and (2) follow from Eqs. (A26) and (A27) for $\chi = 0$ in the limit $\epsilon_i \to 0$. More details of the limit $\epsilon_i \to 0$ are summarized in Appendix B. Equations (1) and (2) describe coupled longitudinal, transverse oscillations for a linearly polarized vector potential. For $a \equiv 0$, they describe nonlinear longitudinal waves; the opposite limit $\phi \equiv 0$ is not possible because of linear polarization. This is in contrast to the circularly polarized case; see Akhiezer and Polovin [3].

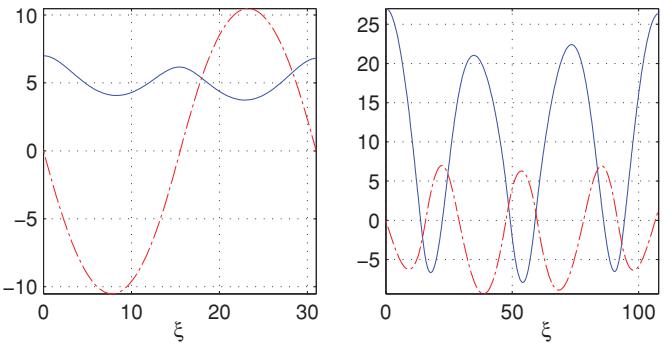

FIG. 2. (Color online) Vector potential a (red dash-dotted line) and scalar potential ϕ (blue solid line) for the solutions labeled a (left) and b (right) in Fig. 1.

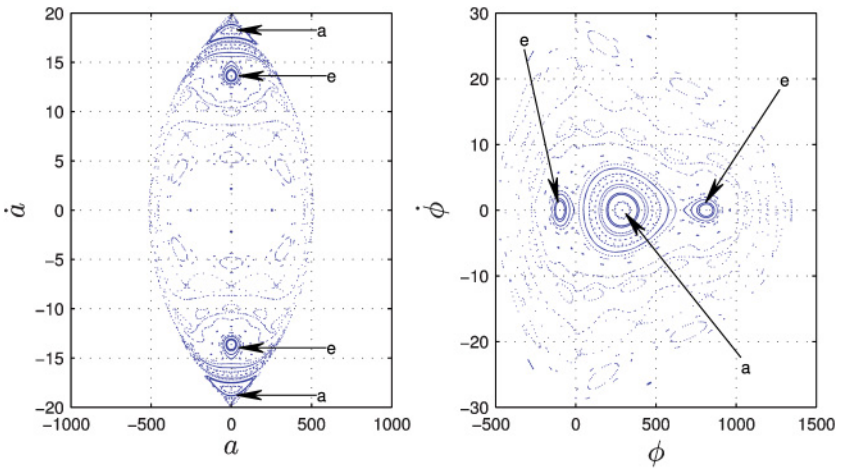

FIG. 3. (Color online) Poincaré surface plot of $\dot{a}$ versus a (for $\phi = \phi_{\min}$) and $\dot{\phi}$ versus ϕ (for $a = 0, \dot{a} > 0$), for $H = 600$ and $\beta = 2$. Labeled are fixed points a,e, corresponding to periodic wave motions.

Within a Lagrangian formulation, Eqs. (1) and (2) follow from the Lagrange density

$$L = (\beta^2 - 1)\frac{\dot{a}^2}{2} + \frac{\dot{\phi}^2}{2} - \frac{\beta}{\beta^2 - 1}(R_e - \beta) + \frac{\phi}{\beta^2 - 1} \equiv L_0. \tag{3}$$

Introducing the canonical momenta

$$p_a \equiv \frac{\partial L}{\partial \dot{a}} = (\beta^2 - 1)\dot{a}, \quad p_\phi \equiv \frac{\partial L}{\partial \dot{\phi}} = \dot{\phi}, \tag{4}$$

we obtain the Hamiltonian

$$H \equiv p_a\dot{a} + p_\phi\dot{\phi} - L = \frac{p_a^2}{2(\beta^2 - 1)} + \frac{p_\phi^2}{2} + \frac{\beta}{\beta^2 - 1}(R_e - \beta) - \frac{\phi}{\beta^2 - 1} \equiv H_0 \equiv T + V_0 \tag{5}$$

for laser intensities and phase velocities β where the ion motion is negligible [22,28]. The dot indicates the derivative with respect to ξ. The canonical equations

$$\dot{a} = \frac{\partial H}{\partial p_a}, \quad \dot{\phi} = \frac{\partial H}{\partial p_\phi}, \quad \dot{p}_a = -\frac{\partial H}{\partial a}, \quad \dot{p}_\phi = -\frac{\partial H}{\partial \phi} \tag{6}$$

are equivalent to (1) and (2). The Hamiltonian formulation is very useful for studying coupled electromagnetic wave solutions. From the canonical equations we conclude $H =$ const. because

$$\frac{dH}{d\xi} = \frac{\partial H}{\partial a}\dot{a} + \frac{\partial H}{\partial \phi}\dot{\phi} + \frac{\partial H}{\partial p_a}\dot{p}_a + \frac{\partial H}{\partial p_\phi}\dot{p}_\phi = 0. \tag{7}$$

The system (1) and (2) is equivalent to the description of Akhiezer and Polovin [3] obtained when studying relativistic plasma motion in coupled longitudinal and transversal electromagnetic waves. Many articles on relativistic plasma wave phenomena used a set of equations equivalent to (1) and (2). However, the range of applicability is limited to a parameter regime where ion motion can be neglected. Certainly for laser amplitudes $a \sim 1/\epsilon_i$ ions can gain relativistic momenta and should be included as mobile species into the model. Since much effort is devoted to pushing laser intensities into and beyond such regimes it seems important to develop an understanding of wave phenomena in plasmas where the ion response may be relativistic. However, one should note that the electrons already become strongly relativistic for $a \sim 1$. Therefore already for $1 < a \ll 1/\epsilon_i$ the electron inertia increases, and the lower mobility of ions becomes less important.

It is possible to calculate the motion of a plasma fluid element by expressing the momenta $\mathbf{p}_\alpha$ in terms of the potentials. In general the motion of a fluid element consists of an average drift in propagation direction of the wave and a superposed motion in the frame where the average momenta are zero. A systematic discussion of plasma motion in linearly polarized periodic waves assuming an electron plasma with immobile ions can be found in Refs. [3,11,22] and will not be repeated here.

III. INFLUENCE OF MOBILE IONS ON STATIONARY WAVE SOLUTIONS

We will now generalize to a plasma consisting of electrons and *mobile* ions. For demonstration we use the largest value of ϵ_i, i.e., $\epsilon_i = 1/1836$. The equations of motion follow from Appendix A for $\chi = 0$ in the form

$$\frac{\partial^2 a}{\partial \xi^2} = -a\frac{\beta}{\beta^2 - 1}\left(\frac{1}{R_e} + \epsilon_i\frac{1}{R_i}\right), \tag{8}$$

$$\frac{\partial^2 \phi}{\partial \xi^2} = \frac{-\beta}{\beta^2 - 1}\left(\frac{\psi_e}{R_e} - \frac{\psi_i}{R_i}\right). \tag{9}$$

They can be derived from the Lagrangian

$$L = \frac{\beta^2 - 1}{2}\dot{a}^2 + \frac{\dot{\phi}^2}{2} + \frac{\beta}{1 - \beta^2}\left(R_e - \beta + \frac{R_i - \beta}{\epsilon_i}\right). \tag{10}$$

Introducing canonical momenta in the same way as above, we find the Hamiltonian

$$H = \frac{p_a^2}{2(\beta^2 - 1)} + \frac{p_\phi^2}{2} + \frac{\beta}{\beta^2 - 1}\left(R_e - \beta + \frac{R_i - \beta}{\epsilon_i}\right). \tag{11}$$

Compared to the immobile ion approximation, we have a perturbed Hamiltonian

$$H = H_0 + \Delta H, \quad H_0 = T + V_0, \quad \Delta H = \frac{\beta}{\beta^2 - 1}\left(\frac{R_i - \beta}{\epsilon_i} + \frac{\phi}{\beta}\right). \tag{12}$$

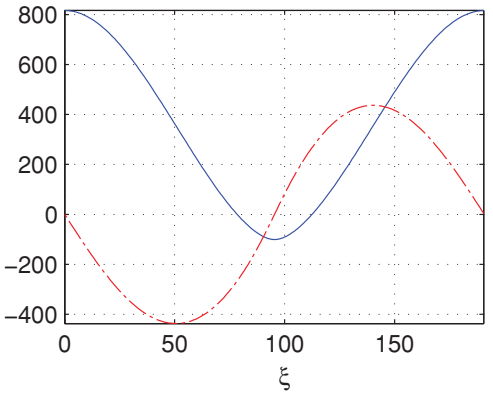

FIG. 4. (Color online) Vector potential a (red dash-dotted line) and scalar potential ϕ (blue solid line) for the solution e in Fig. 3

Clearly (see Appendix B)

$$\Delta H \to 0 \quad \text{for} \quad \epsilon_i \to 0. \tag{13}$$

But for fixed $\epsilon_i \ll 1$

$$\Delta H \ll V_0 \quad \text{only for} \quad \max(a) \to 0. \tag{14}$$

On the other hand, when the laser amplitude a becomes larger, even for small ϵ_i the "perturbation" ΔH cannot be neglected anymore compared to the zeroth-order Hamiltonian.

In order to study the variety of possible solutions of Eqs. (8) and (9) at fixed values of H, corresponding to the energy of the coupled electromagnetic, electrostatic oscillation, and β, we render Poincaré section plots of the four-dimensional phase space. Equations (8) and (9) are nonlinearly coupled oscillators, which can be solved by standard Runge-Kutta algorithms. In produce phase-space projections we will use one oscillator as a clock while plotting the other one every time the clock ticks. Using a as a clock, ticking every time when $a = 0$ and $\dot{a} > 0$ we will plot ϕ versus $\dot{\phi}$. When using ϕ as a clock we will plot a versus $\dot{a}$ every time when $\dot{\phi} = 0$ and $\ddot{\phi} > 0$. With the help of these projections it is easy to identify periodic solutions as they correspond to fixed points or island chains. The latter show characteristic amplitude modulations [14]. The initial conditions for all trajectories are such that we require $a = 0, \dot{\phi} = 0$ at $\xi = 0$.

Figure 1 shows Poincaré section plots for $\beta = 2$ and $H = 10$. We labeled three periodic solutions a–c in the plots. Solution a is the famous figure-eight solution, having an electromagnetic field oscillating with twice the frequency of the electrostatic field. The island chains b and c correspond to higher-order amplitude-modulated solutions. It is interesting to note that one obtains qualitatively the same types of solutions as the ones appearing in the Akhiezer-Polovin model [22]. Of course, a detailed quantitative comparison of the phase-space structures reveals small changes. But the conclusion is that for the chosen parameter regime the ion motion is still negligible.

Typical forms for the vector and scalar potentials for $\beta = 2$ and $H = 10$ are shown in Fig. 2, revealing that the solutions predicted by the Poincaré plots are truly periodic. The left diagram depicts the potentials for the figure-eight solution a while the right diagram shows the potentials for a solution of type b. From here we can read off the typical magnitudes, showing that the maximum amplitudes of a are of the order of 10. Hence we have already ultrarelativistic electron motion but almost nonrelativistic ions. The immobile ion approximation is still quite good at these magnitudes of a and ϕ, as can be concluded from a comparison with previous studies [22].

Next, we further increase the energy H. With increasing energies more and more formerly closed Kolmogorov-Arnold-Moser (KAM) surfaces break up and form island chains. For $H = 600$, the phase-space topology has changed significantly; very pronounced new fixed points appear. Figure 3 demonstrates the becoming of a new fixed point, labeled e. The new fixed points e correspond to fields shown in Fig. 4. The solutions a and ϕ are of the same magnitude and share a frequency. Although electrons are strongly relativistic, ions are still weakly relativistic. The according plasma motion is a circular trajectory in the average drift frame. Besides the creation of the new fixed points, we observe an increase in the amount of island chains.

Let us discuss whether the change in phase-space topology, and thereby the appearance of new solutions e, should be attributed to ion motion. For that we carried out Poincaré plots for the same values $\beta = 2$ and $H = 600$, however, using the Hamiltonian (5) for fixed ions. Figure 5 shows that the solution e does not appear in the case of immobile ions.

A sense of caution is, however, appropriate here. As long as the energy is not too large, and depending on the choice

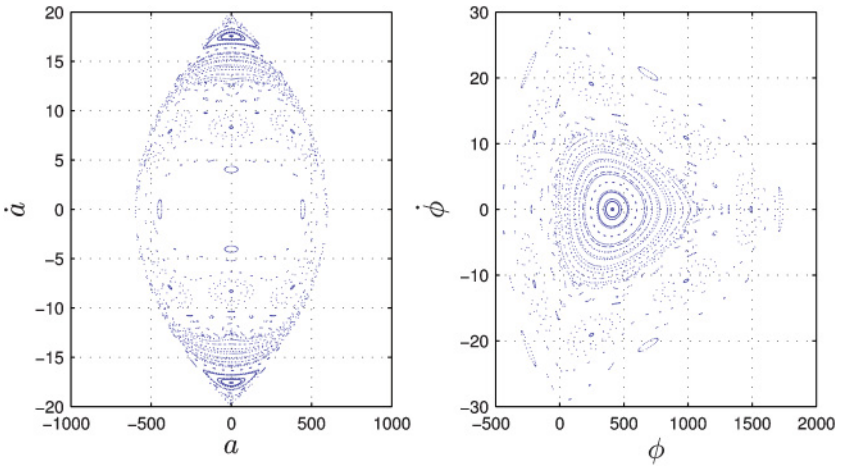

FIG. 5. (Color online) Poincaré surface plot of $\dot{a}$ versus a (for $\phi = \phi_{\min}$) and $\dot{\phi}$ versus ϕ (for $a = 0, \dot{a} > 0$), for $H = 600$ and $\beta = 2$. The ion motion has been neglected here. Notice the different structure of the phase space compared to Fig. 3.

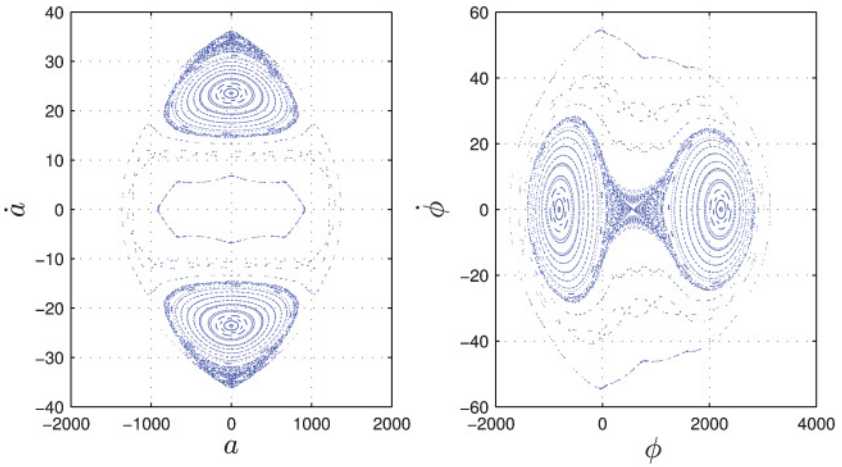

FIG. 6. (Color online) Poincaré surface plot of $\dot{a}$ versus a (for $\phi = \phi_{\min}$) and $\dot{\phi}$ versus ϕ (for $a = 0, \dot{a} > 0$), for $H = 2000$ and $\beta = 2$ with mobile ions.

of the other control parameter β, solutions of type e can also be observed in systems consisting of electrons with a fixed ion background. Regimes for solutions e were detected in Refs. [11,14,22]. For example, a phase-space structure similar to the one shown in Fig. 3 can be found at $\beta = 2.5$ and $H = 100$ for a system with immobile ions. In the latter case the separatrix that is formed around the islands containing a and e is a closed KAM surface [29]. Then the ion motion leads to a stochastization of the separatrix and the vanishing of hyperbolic fixed points along the separatrix.

Hyperbolic fixed points represent (deformed) figure-eight motions [22]. With increasing H the volume contained by the central island containing the fixed-point a becomes smaller, while the volumes of the islands around the fixed points e grow. At higher intensities the ion motion becomes strongly relativistic ($\epsilon_i \phi > 1$). We observe that with increasing energy the islands around the fixed point a shrink, while the islands around solution e grow. The process continues with increasing values of H, until only the islands of e are left, separated by a stochastic separatrix. Figure 6 shows Poincaré section plots for $\beta = 2$ and $H = 2000$. Compared to Fig. 3 the fixed point corresponding to solution a does not exist anymore. Solutions of type e and higher-order amplitude modulated solutions are still existent. This is a generic result. Strongly ultrarelativistic plasmas do not show the figure-eight solution anymore. The manifold of solutions becomes relatively simple. In addition to the higher-order amplitude modulated solutions that occupy little phase space, the circular motion and the surrounding island are the dominating surviving structures.

IV. SIMILARITY TO ELECTRON-POSITRON PLASMAS

A. Effective masses

When H becomes large and the typical amplitude a approaches $1/\epsilon_i$, electrons quivering in the strongly ultrarelativistic waves effectively become heavy. The quantitative differences in effective masses between electrons and ions are expected to diminish. In the present section we quantify that scenario for relativistic plasma waves.

Electron and ion motion within the relativistic waves follows from the solutions (A16) and (A17) for the parallel component together with $\mathbf{p}_{\alpha\perp} = q_\alpha \mathbf{A}_\perp$ for the perpendicular component. The velocities are varying, depending on the position in the wave. Then also the relativistic γ factor changes with ξ. We obtain the relativistic γ factor via expression (A25). Typical examples for γ_e and γ_i at large wave energies are shown in Fig. 7.

Because of the variations with ξ, we should average γ over one oscillation period for obtaining an averaged γ factor. After multiplication with the corresponding rest mass, the averaged effective masses can be calculated. We have evaluated the averaged effective masses for a series of waves. Depending on the Hamiltonian H the graphs shown in Fig. 8 appear. The effective electron-to-ion mass ratio is altered by relativistic effects in such a way that the ratio increases with higher intensities. For $H \to \infty$ the effective mass ratio $m_e\langle\gamma_e\rangle / m_i\langle\gamma_i\rangle \to 1$. However, for large H quantum effects, ignored in the present formulation, will enter into the picture. Quantum effects become important when the photons being generated due to Compton scattering have energies of the order of the electron energy $\gamma_e m_e c^2$. The frequency of the photon being generated by an electron oscillating with frequency ω is $\omega_n = \gamma_e^3 \omega$. From here we may estimate that for $\gamma_e \geqslant \mathcal{O}(10^3)$ (when using wavelength $\lambda = 1\mu$m) quantum effects come into play, and the purely classical treatment breaks down. At $\lambda = 1\mu$m the condition for quantum effects may be translated into the condition $a \geqslant \mathcal{O}(10^3)$ for the amplitude a. These estimates show that at least up to $H \leqslant \mathcal{O}(2 \times 10^3)$ the present classical treatment will apply. That is exactly the range that we investigated above. Of course, radiation damping that already

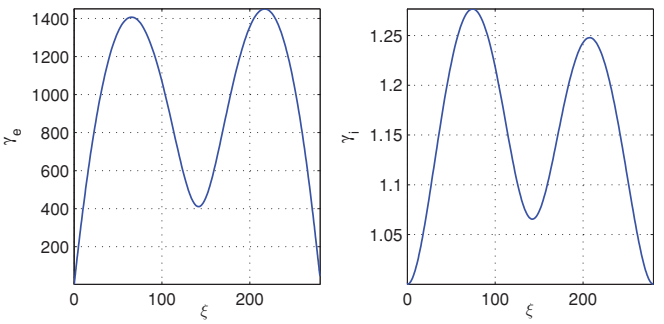

FIG. 7. (Color online) The relativistic γ factors γ_e and γ_i calculated from (A25) for a specific wave solution with $\beta = 2, H = 2000$.

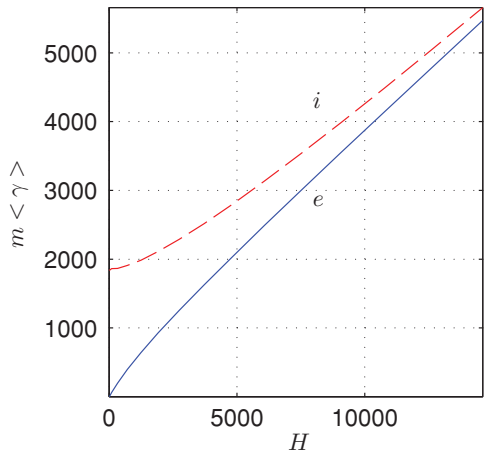

FIG. 8. (Color online) Averaged effective masses $m\langle\gamma\rangle \hat{=} m_\alpha\langle\gamma_\alpha\rangle$ of electrons ($\alpha = e$) and ions (protons) ($\alpha = i$) as functions of H for $\beta = 2$.

might set in at lower values is not taken into account within the Hamiltonian formulation.

B. Electron-positron plasma

The results for ultrarelativistic electron-ion plasmas suggest that for high intensities the electron-ion system behaves qualitatively like a electron-positron plasma. The analogy to an electron-positron plasma with respect to the topology of the phase space will be worked out in the following to support this expectation. Pair plasmas have attracted special attention mainly because of the enormous astrophysical applications [30].

Setting $\chi = 1$ in the basic formulas (A26) and (A27) of Appendix A, we obtain the equations of motion for an electron-positron plasma

$$\frac{d^2a}{d\xi^2} = -a\frac{\beta}{\beta^2-1}\left(\frac{1}{R_e}+\frac{1}{R_p}\right), \tag{15}$$

$$\frac{d^2\phi}{d\xi^2} = \frac{-\beta}{\beta^2-1}\left(\frac{\psi_e}{R_e}-\frac{\psi_p}{R_p}\right). \tag{16}$$

They follow from the Lagrangian

$$L = \frac{\beta^2-1}{2}\dot{a}^2 - \frac{\dot{\phi}^2}{2} + \frac{\beta}{\beta^2-1}(R_e - \beta + R_p - \beta). \tag{17}$$

The corresponding Hamiltonian is

$$H = \frac{p_a^2}{2(\beta^2-1)} + \frac{p_\phi^2}{2} - \frac{\beta}{\beta^2-1}(R_e - \beta + R_p - \beta). \tag{18}$$

Typical Poincaré section plots of $\dot{a}$ versus a and $\dot{\phi}$ versus ϕ for electron-positron plasma at low energies are shown in Fig. 9. We recognize the strong similarity with Fig. 6. That means that the expected similarity of an ultrarelativistic electron-ion plasma with a relativistic electron-positron plasma is endorsed.

C. Bifurcation scenario

We can mimic the reported bifurcation scenario for ultrarelativistic electron-ion plasmas up to the agreement in phase space for large energies (when H is the control parameter) by considering an electron-ion-positron plasma [31]. For that purpose we discuss now the influence of positrons (with control parameter $0 < \chi \leqslant 1$) on a relativistic wave solution. Positrons carry the same amount of positive charge as we considered for the ions, but they have the same mass as the electrons. This implies that nonlinearities due to positrons appear on the same scale as they do for electrons. The general Hamiltonian corresponding to Eqs. (A26) and (A27) is

$$H = \frac{p_a^2}{2(\beta^2-1)} + \frac{p_\phi^2}{2} + \frac{\beta}{\beta^2-1}\left[R_e - \beta + \chi(R_p-\beta) + (1-\chi)\frac{R_i-\beta}{\epsilon_i}\right]. \tag{19}$$

That will be used for the following discussion.

The presence of positrons leads to a reduction of the maximum value of ϕ at a fixed maximum value of a since the positrons can react more strongly to the radiation pressure than the heavier ions. This, for example, is known to influence the possibility of having localized solutions in a system consisting only of electrons and positrons [32].

To demonstrate that the positrons already have a pronounced impact for low positron density, we present four Poincaré plots in Fig. 10. The plasma is assumed to be neutral, hence we adjust the ratio of positron to ion density. We show

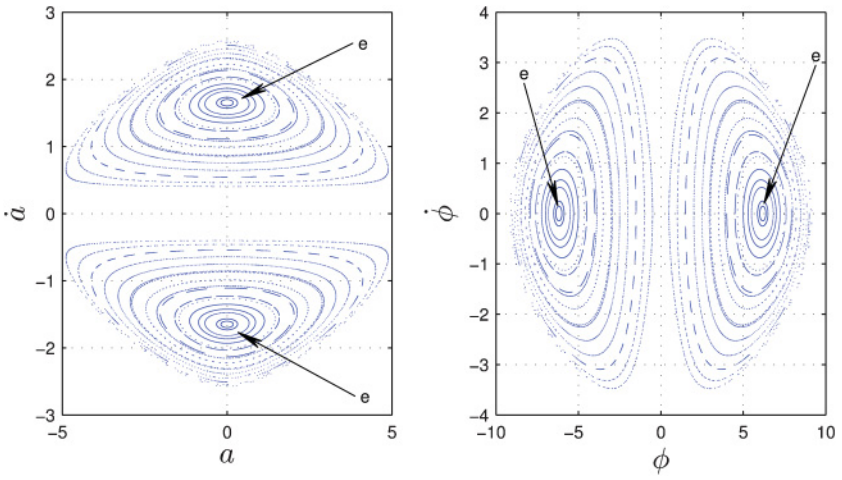

FIG. 9. (Color online) Poincaré section plots of $\dot{a}$ versus a and $\dot{\phi}$ versus ϕ for electron-positron plasmas with $H = 10$ and $\beta = 2$.

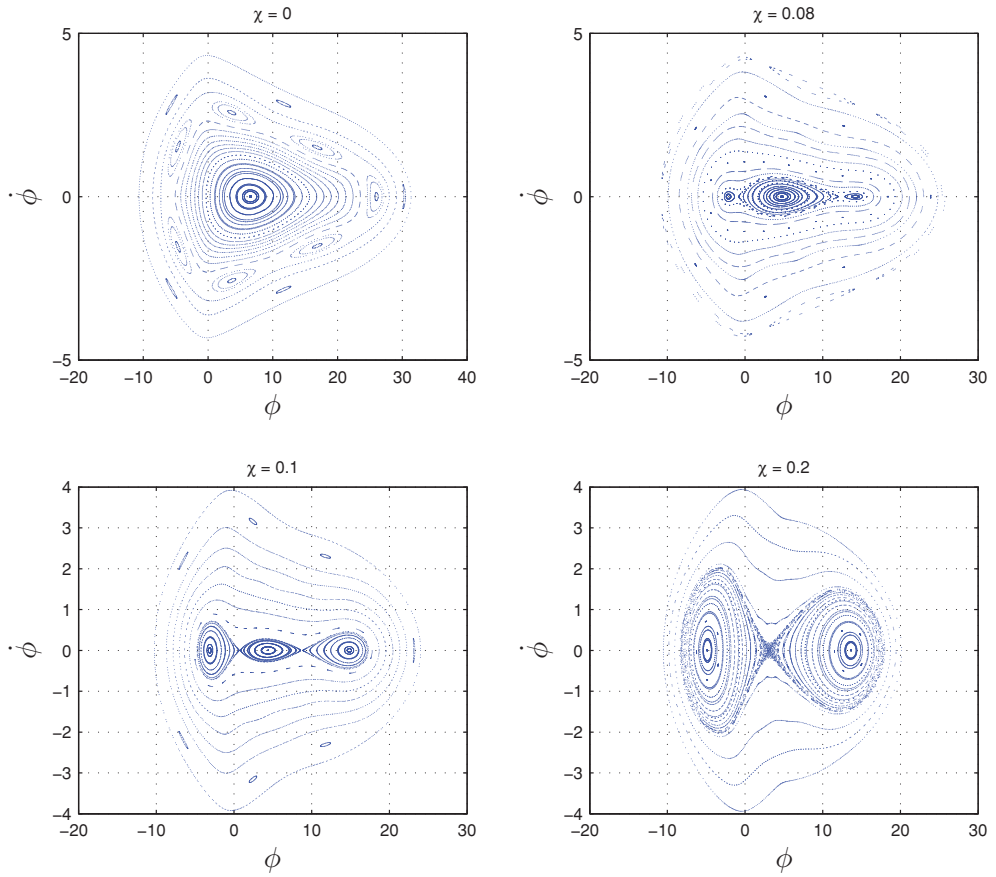

FIG. 10. (Color online) Poincaré section plots of $\dot{\phi}$ versus ϕ for electron-positron-ion plasmas with $H = 10$ and $\beta = 2$. The four figures refer to different ion density to positron density ratios of $\chi = 0$, 0.08, 0.1, and $\chi = 0.2$, respectively.

results for $\chi = 0$, 0.08, 0.1 and $\chi = 0.2$, respectively. The plots are done for $H = 10$ and $\beta = 2$. Figure 9 adds the case $\chi = 1$. Ions are included in the calculations, but as the average field intensities are very low, ion motion is not significant.

With increasing positron density we observe a transition from a single fixed-point topology (Fig. 10, upper left frame, no positrons present) to a system with two different fixed points (Fig. 10, lower right frame, where 20% of all positive charge is carried by positrons). The two remaining fixed points are (similar to the electron-ion system at higher intensities) separated by a stochastic separatrix. In the intermediate regime $0.07 < \chi < 0.2$ we observe an interval where all three solutions are present at the same time. Increasing the positron density even more (thus replacing more heavy ions by lighter positrons) does not seem to lead to further qualitative changes in the phase-space structure; see Fig. 9. However, it is notable that even a small amount of positrons can affect the behavior of the system. The actual positron-to-ion density ratio needed to influence the phase-space structure depends on the plasma density, which is increasing with increasing phase velocity β. For $\beta \to 1$ we observe that already a positron density of 1% can lead to a bifurcation similar to the one demonstrated in Fig. 10.

Summarizing, when comparing electron-ion plasmas (with control parameter H) with electron-ion-positron plasmas (with control parameter χ) we observe similar bifurcation scenarios. The phase-space topologies are very much alike when we alter the control parameters.

V. SUMMARY AND CONCLUSION

We studied the existence of stationary, linearly polarized, coupled electrostatic and electromagnetic waves in ultrarelativistic electron-ion plasmas. Making use of the Hamiltonian nature of the problem, considering the potentials a and ϕ as canonical variables, we discussed the phase-space topology of the system in dependence of the control parameter H. Rendering Poincaré section plots allows to study the influence of ion mobility on the phase-space structure. We identified periodic solutions in different energy regimes by discussing fixed points.

When considering the fully relativistic electron-ion plasma ($\chi = 0, \epsilon_i = 1/1836$), in the limit of low energies one recovers known periodic relativistic wave solutions, such as figure-eight, circular motion, and higher-order amplitude-modulated fields [3,11,22,28]. The immobile ion approximation is good for low energies.

Increasing the energy so that the ions become weakly relativistic, we observed a change in the structure of the phase space. The ions start reacting to the radiation pressure and decrease the maximum electrostatic potential one can obtain at a fixed value of H. This mechanism influences the coupling of a and ϕ and results in a reduction of the phase-space volume around the fixed point (labeled a) associated with the figure-eight plasma motion. At the same time new islands are generated in the Poincaré plots with new elliptic fixed points

(labeled e) corresponding to periodic solutions. This process continues with increasing energy. The island containing fixed point a keeps shrinking until only a stochastic volume is left. We conclude that the ion dynamics strongly affect the structure of the phase space. Ion motion must not be neglected in the high-intensity regime. The inclusion of ion mobility influences the manifold of stationary wave solutions with linear polarization and changes the structure of the phase space. The changes in the topology of the Poincaré section plots indicate that the nature of the solutions changes qualitatively, not only quantitatively. We have reported the bifurcation from figure-eight to circular motion.

As an interesting perspective, the availability of high-power lasers will permit researchers in the future to simulate in laboratory experiments with conventional electron-ion plasmas many aspects of the physics of astrophysical electron-positron plasmas.

ACKNOWLEDGEMENT

This work was performed under the auspices of the DFG-supported project "SFB TR-18."

APPENDIX A: DERIVATION OF THE EQUATIONS OF MOTION

Here the one-dimensional (1D) relativistic Maxwell two-fluid model is the starting point for considering high-frequency wave motion of an electron-ion plasma in the hydrodynamical approximation. The 1D propagation geometry for the waves means that all quantities vary only along the direction of propagation, let us say x. Vector quantities, of course, may have components pointing in other directions than x. The plasma is assumed to be cold, so kinetic effects are neglected. For later interpretations, here we formulate the system with a slight generalization to a three-species plasma consisting of electrons (e), ions (i), and positrons (p) using the index $\alpha = e,i,p$. Dimensionless quantities are introduced in the usual way, i.e., lengths x, times t, velocities $\mathbf{v}_\alpha$, momenta $\mathbf{p}_\alpha$, vector $\mathbf{A}$, and scalar potential ϕ, and particle densities n_α are normalized by c/ω_{pe}, ω_{pe}^{-1}, c, $m_e c$, $m_e c/e$, $m_e c^2/e$, and n_0, respectively. Here $\omega_{pe} = (n_{e0}e^2/\epsilon_0 m_e)^{1/2}$ is the electron plasma frequency, m_e the electron rest mass, e the (absolute value of the) electron charge, and n_{e0} the unperturbed electron density. Charges q_α are normalized to $-e$, so $q_e = 1, q_i = q_p = -1$; masses are normalized by m_e. In order to ensure global charge neutrality we introduce the proton-to-ion density ratio $\chi = n_{0p}/n_{0i}$ such that $n_{0e} = (1-\chi)n_{0i} + \chi n_{0p}$. Maxwell's equations (in SI units) will be expressed in the Coulomb gauge, which leads to $\mathbf{A} \equiv \mathbf{A}_\perp$ as a result of the 1D propagation model. A further consequence of the 1D geometry is that $\mathbf{p}_{\alpha\perp} = q_\alpha \mathbf{A}_\perp$. The hydrodynamic equations for the particle densities n_α and the (parallel) momentum p_α, as well as the Maxwell equations for the vector and scalar potentials $\mathbf{A}_\perp$ and ϕ, can be written in dimensionless form as

$$\frac{\partial^2 \mathbf{A}_\perp}{\partial x^2} - \frac{\partial^2 \mathbf{A}_\perp}{\partial t^2} = \sum_\alpha q_\alpha \epsilon_\alpha \frac{n_\alpha}{\gamma_\alpha} \mathbf{p}_{\alpha\perp}, \tag{A1}$$

$$\frac{\partial^2 \phi}{\partial x^2} = \sum_\alpha q_\alpha n_\alpha, \tag{A2}$$

$$\frac{\partial^2 \phi}{\partial t \partial x} + \sum_\alpha q_\alpha \epsilon_\alpha \frac{n_\alpha p_\alpha}{\gamma_\alpha} = 0, \tag{A3}$$

$$\frac{\partial n_\alpha}{\partial t} + \epsilon_\alpha \frac{\partial}{\partial x}\left(\frac{n_\alpha p_\alpha}{\gamma_\alpha}\right) = 0, \tag{A4}$$

$$\frac{\partial p_\alpha}{\partial t} = \frac{\partial}{\partial x}\left(q_\alpha \phi - \frac{\gamma_\alpha}{\epsilon_\alpha}\right), \tag{A5}$$

where $\epsilon_\alpha = m_e/m_\alpha$. The normalized (rest) masses are $m_e = m_p = 1$ and $m_i = 1836$ (when the ions are protons). The relativistic γ factors are $\gamma_\alpha = \sqrt{1 + \epsilon_\alpha^2(|\mathbf{A}_\perp|^2 + p_\alpha^2)}$ for the different species α.

Transforming to a frame of reference moving with the normalized phase velocity $\beta = v/c \gg 1$ of an electromagnetic wave, by introducing $\xi = x - \beta t$ one gets

$$(1-\beta^2)\frac{\partial^2 \mathbf{A}_\perp}{\partial \xi^2} - \frac{\partial^2 \mathbf{A}_\perp}{\partial t^2} + 2\beta \frac{\partial^2 \mathbf{A}_\perp}{\partial \xi \partial t} = \sum_\alpha q_\alpha \epsilon_\alpha \frac{n_\alpha}{\gamma_\alpha} \mathbf{p}_{\alpha\perp}, \tag{A6}$$

$$\frac{\partial^2 \phi}{\partial \xi^2} = \sum_\alpha q_\alpha n_\alpha, \tag{A7}$$

$$\frac{\partial}{\partial \xi}\left(\frac{\partial}{\partial t} - \beta \frac{\partial}{\partial \xi}\right)\phi + \sum_\alpha q_\alpha \epsilon_\alpha \frac{n_\alpha p_\alpha}{\gamma_\alpha} = 0, \tag{A8}$$

$$\frac{\partial n_\alpha}{\partial t} + \frac{\partial}{\partial \xi}\left(\epsilon_\alpha \frac{n_\alpha p_\alpha}{\gamma_\alpha} - \beta n_\alpha\right) = 0, \tag{A9}$$

$$\frac{\partial p_\alpha}{\partial t} - \beta \frac{\partial p_\alpha}{\partial \xi} = \frac{\partial}{\partial \xi}\left(q_\alpha \phi - \frac{\gamma_\alpha}{\epsilon_\alpha}\right). \tag{A10}$$

The linear dispersion relation suggests $\beta \to 1$ when the plasma density approaches zero, whereas $\beta \to \infty$ occurs when one approaches the critical density. In the new frame of reference we will discuss stationary solutions. Then all quantities depend only on ξ and not explicitly on t (effectively meaning $\partial/\partial t = 0$). We therefore start from

$$(1-\beta^2)\frac{\partial^2 \mathbf{A}_\perp}{\partial \xi^2} = \sum_\alpha q_\alpha \epsilon_\alpha \frac{n_\alpha}{\gamma_\alpha} \mathbf{p}_{\alpha\perp}, \tag{A11}$$

$$\frac{\partial^2 \phi}{\partial \xi^2} = \sum_\alpha q_\alpha n_\alpha, \tag{A12}$$

$$-\beta \frac{\partial^2 \phi}{\partial \xi^2} + \sum_\alpha q_\alpha \epsilon_\alpha \frac{n_\alpha p_\alpha}{\gamma_\alpha} = 0, \tag{A13}$$

$$\frac{\partial}{\partial \xi}\left(\epsilon_\alpha \frac{n_\alpha p_\alpha}{\gamma_\alpha} - \beta n_\alpha\right) = 0, \tag{A14}$$

$$\frac{\partial}{\partial \xi}\left(\beta p_\alpha + q_\alpha \phi - \frac{\gamma_\alpha}{\epsilon_\alpha}\right) = 0. \tag{A15}$$

It is possible to express n_α, p_α, and γ_α as functions of $\mathbf{A}_\perp$ and ϕ. Integrating Eqs. (A14) and (A15), one gets

$$\epsilon_\alpha \frac{n_\alpha p_\alpha}{\gamma_\alpha} = C_{\alpha 1} + \beta n_\alpha \tag{A16}$$

and

$$q_\alpha \phi - \frac{\gamma_\alpha}{\epsilon_\alpha} + \beta p_\alpha = -C_{\alpha 2}. \tag{A17}$$

We determine $C_{\alpha 1}$ by postulating in Eq. (A16) for a uniform plasma $p_\alpha = 0$ at $n_e = 1, n_i = (1-\chi), n_p = \chi$. This results in $C_{e1} = -\beta, C_{i1} = -\beta(1-\chi)$, and $C_{p1} = -\beta\chi$.

Next, inserting

$$\gamma_\alpha = \sqrt{1 + \epsilon_\alpha^2(|\mathbf{A}_\perp|^2 + p_\alpha^2)} \tag{A18}$$

into Eq. (A17) we obtain a quadratic equation for p_α,

$$1 + \epsilon_\alpha^2\left(|\mathbf{A}_\perp|^2 + p_\alpha^2\right) = \epsilon_\alpha^2(q_\alpha\phi + \beta p_\alpha + C_{\alpha 2})^2. \tag{A19}$$

We determine $C_{\alpha 2}$ in such a way that $\phi = 0$, where $p_\alpha = 0$ and $|\mathbf{A}_\perp| = a_0$. With this calibration we get

$$C_{\alpha 2} = \sqrt{\frac{1}{\epsilon_\alpha^2} + a_0^2}. \tag{A20}$$

Defining

$$\psi_\alpha = \epsilon_\alpha(q_\alpha\phi + C_{\alpha 2}), \tag{A21}$$

$$R_\alpha = \left[\psi_\alpha^2 - (1-\beta^2)\left(1 + \epsilon_\alpha^2 a^2\right)\right]^{1/2}, \tag{A22}$$

we find

$$p_\alpha = \frac{\beta\psi_\alpha - R_\alpha}{\epsilon_\alpha(1-\beta^2)}, \tag{A23}$$

$$n_\alpha = \frac{C_{\alpha 1}(\psi_\alpha - \beta R_\alpha)}{R_\alpha(\beta^2 - 1)}, \tag{A24}$$

$$\gamma_\alpha = \frac{\psi_\alpha - \beta R_\alpha}{1-\beta^2}. \tag{A25}$$

When focusing on linearly polarized waves, we introduce $\mathbf{A}_\perp = a\hat{\mathbf{e}}_z$. We end up with the following two coupled differential equations for the (normalized) potentials a and ϕ:

$$\frac{d^2a}{d\xi^2} = -a\frac{\beta}{\beta^2-1}\left[\frac{1}{R_e} + \frac{\chi}{R_p} + \epsilon_i\frac{1-\chi}{R_i}\right], \tag{A26}$$

$$\frac{d^2\phi}{d\xi^2} = \frac{-\beta}{\beta^2-1}\left[\frac{\psi_e}{R_e} - \chi\frac{\psi_p}{R_p} - (1-\chi)\frac{\psi_i}{R_i}\right]. \tag{A27}$$

Equations (A26) and (A27) describe the nonlinear relativistic coupling between transverse and longitudinal oscillations. They are very similar to the basic equations for the dynamics of relativistic solitons [33,34] The system (A26) and (A27) constitutes the starting point for the present investigation; it can be derived from an Hamiltonian as is discussed in the main part of the paper.

APPENDIX B: THE IMMOBILE ION APPROXIMATION

In the limit $\epsilon_i \to 0$ the following limits can be calculated for finite a:

$$\psi_i \to 1, \quad R_i \to \beta, \quad C_{i2} \to \frac{1}{\epsilon_i}, \tag{B1}$$

$$\frac{\psi_i}{R_i} \to \frac{1}{\beta}, \quad \frac{R_i - \beta}{\epsilon_i} \to -\frac{\phi}{\beta}. \tag{B2}$$

They are useful for the reduction of the problem with full ion dynamics to the model with immobile ions.

It is interesting to note that the same limiting values are obtained for finite ϵ_i, e.g., $\epsilon_i = 1/1836$ in the limit $a \to 0$. This shows that in the weakly relativistic limit the immobile ion approximation is applicable. However, for large laser amplitudes $a \gg 1$, the ion motion has to be taken into account even for $\epsilon_i = 1/1836$.

[1] A. Pukhov, Rep. Prog. Phys. **66**, 47 (2003).
[2] G. A. Mourou, T. Tajima, and S. V. Bulanov, Rev. Mod. Phys. **78**, 309 (2006).
[3] A. I. Akhiezer and R. V. Polovin, Sov. Phys. JETP **3**, 696 (1956) [Zh. Eksp. Teor. Fiz. **30**, 915 (1956)].
[4] J. M. Dawson, Phys. Rev. **113**, 383 (1959).
[5] P. Kaw and J. Dawson, Phys. Fluids **13**, 472 (1970).
[6] E. S. Sarachik and G. T. Schappert, Phys. Rev. D **1**, 2738 (1970).
[7] C. Max and F. Perkins, Phys. Rev. Lett. **27**, 1342 (1971).
[8] A. C.-L. Chian and P. C. Clemmow, J. Plasma Phys. **14**, 505 (1975).
[9] C. E. Max, Phys. Fluids **16**, 1277 (1973).
[10] W. Lunow, Plasma Phys. **10**, 879 (1968).
[11] T. C. Pesch and H.-J. Kull, Phys. Plasmas **14**, 083103 (2007).
[12] P. C. Clemmow and R. D. Harding, J. Plasma Phys. **23**, 71 (1980).
[13] P. C. Clemmow, J. Plasma Phys. **27**, 177 (1982).
[14] N. Bisai, A. Sen, and K. Jain, J. Plasma Phys. **56**, 209 (1996).
[15] T. C. Pesch and H. J. Kull, Laser Phys. **19**, 1753 (2009).
[16] T. C. Pesch and H.-J. Kull, Europhys. Lett. **85**, 25003 (2009).
[17] B. He, T.-Q. Chang, and J. Liu, Phys. Plasmas **16**, 023102 (2009).
[18] T. C. Pesch and H.-J. Kull, Phys. Plasmas **17**, 012305 (2010).
[19] B. Grammaticos, A. Ramani, and H. Yoshida, Phys. Lett. A **124**, 65 (1987).
[20] D. Teychenné, E. Bésuelle, A. Oloumi, and R. R. E. Saloma, Phys. Rev. Lett. **85**, 5571 (2000).
[21] A. Bourdier, Physica D **238**, 226 (2009).
[22] G. Lehmann and K. H. Spatschek, Phys. Plasmas **17**, 072102 (2010).
[23] O. Shiryaev, Phys. Plasmas **13**, 112304 (2006).
[24] O. Shiryaev, Phys. Plasmas **15**, 012308 (2008).
[25] G. Lehmann, E. W. Laedke, and K. H. Spatschek, Phys. Plasmas **13**, 092302 (2006).
[26] G. Lehmann, E. W. Laedke, and K. H. Spatschek, Phys. Plasmas **14**, 103109 (2007).
[27] G. Lehmann, E. W. Laedke, and K. H. Spatschek, Phys. Plasmas **15**, 072307 (2008).
[28] P. Kaw, A. Sen, and E. Valeo, Physica D **9**, 96 (1983).
[29] V. Saxena, A. Sen, and P. Kaw, Phys. Rev. E **80**, 016406 (2009).
[30] S. M. Mahajan, N. L. Shatashvili, and V. I. Berezhiani, Phys. Rev. E **80**, 066404 (2009).
[31] A. Sharma, I. Kourakis, and P. K. Shukla, Phys. Rev. E **82**, 016402 (2010).
[32] V. I. Berezhiani, M. Y. El-Ashry, and U. A. Mofiz, Phys. Rev. E **50**, 448 (1994).
[33] D. Farina and S. V. Bulanov, Phys. Rev. Lett. **86**, 5289 (2001).
[34] D. Farina and S. Bulanov, Plasma Phys, Control. Fusion **47**, A73 (2005).